Drag coefficient Uncertainty for floating wind turbines

Fabien Robaux, Adria Borras Nadal, Christophe Peyrard, Michel Benoit, William Benguigui, Martin Guiton

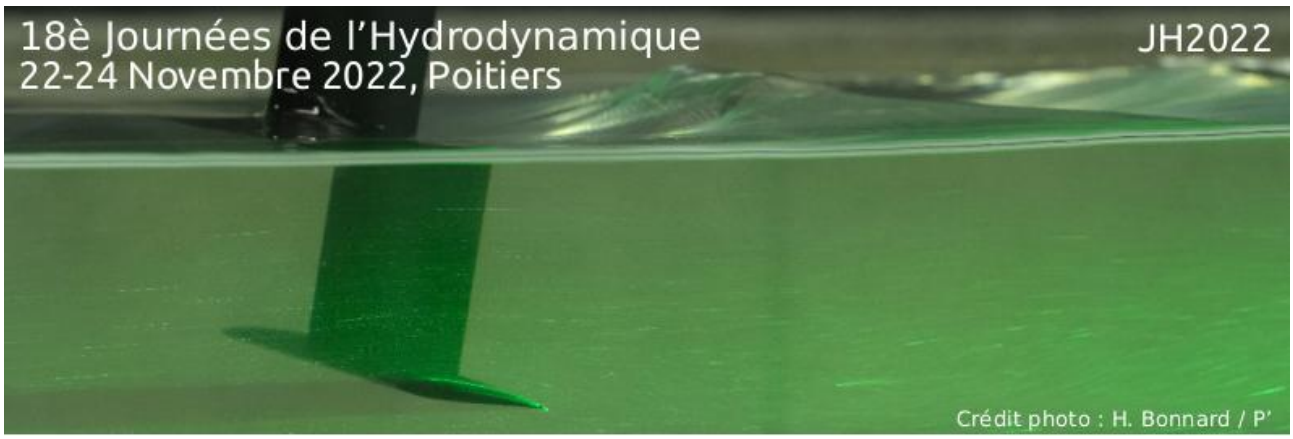

DRAG COEFFICIENT UNCERTAINTY FOR FLOATING WIND TURBINES

Fabien ROBAUX [(1,2)*], Adria BORRAS NADAL [(3)], Christophe PEYRARD [(1,2)], Michel BENOIT [(1,2)], William BENGUIGUI [(4,5)], Martin GUITON [(6)]

[*] *fabien.robaux@edf.fr*

[(1)] Saint-Venant Hydraulics Laboratory (Ecole des Ponts ParisTech, EDF R&D), Chatou, France
[(2)] EDF R&D, Laboratoire National d'Hydraulique et Environnement (LNHE), Chatou, France
[(3)] IFP Energies nouvelles (IFPEN), Rueil-Malmaison, France
[(4)] EDF R&D, Dept. Mécanique des Fluides, Energies et Environnement (MFEE), Chatou, France
[(5)] IMSIA, UMR 9219 EDF/CNRS/CEA/ENSTA ParisTech, Palaiseau, France
[(6)] IFP Energies nouvelles (IFPEN), Solaize, France

Résumé

La détermination des coefficients hydrodynamiques d'un objet soumis à un champ de vagues est un enjeu majeur du design des structures offshore. On étudie et valide ici la capacité d'extraction de ces coefficients à partir de simulations CFD (neptune_cfd, EDF R&D et OpenFoam®, IFPEN). Une attention particulière est portée sur les coefficients de traînée, C_d, critiques en termes d'effets physiques, et qui ne peuvent être obtenus par les simulations potentielles linéaires, largement utilisées aujourd'hui dans l'industrie. Une comparaison code à code est effectuée sur plusieurs corps simples soumis à différentes conditions de vague, pour valider non seulement les séries temporelles d'efforts obtenues, mais aussi comparer les coefficients hydrodynamiques extraits avec les données de la littérature. Une étude prospective est ensuite réalisée dans le cadre d'un flotteur complet, dont plusieurs sections caractéristiques sont sélectionnées et analysées, toujours avec l'objectif d'obtenir une représentation en C_d de l'ensemble du flotteur.

Summary

The determination of the hydrodynamic coefficients of an object subjected to a wave field is a major issue in the design of offshore structures. The ability to extract these coefficients from CFD simulations (neptune_cfd, EDF R&D and OpenFoam®, IFPEN) is studied and validated here. Particular attention is paid to the drag coefficients, C_d, which are critical in terms of physical effects, but which cannot be obtained from linear potential simulations, widely used nowadays in the industry sector. A code-to-code comparison is performed on several simple bodies subjected to a wide range of wave conditions, to validate not only the time series of forces obtained, but also to compare the hydrodynamic coefficients obtained with data from the literature. A prospective study is then carried out on a complete floater, from which several characteristic sections are selected and analyzed, always with the objective of obtaining a C_d representation of the whole floater.

I – Introduction

The European Union (EU) has set an ambitious target of 300 GW installed capacity of offshore wind power in the EU by 2050 [1]. To achieve this goal, Floating Offshore Wind Turbine (FOWT) systems are currently under development for future cost-effective offshore wind farms. The project HIPERWIND (HIghly advanced Probabilistic design and Enhanced Reliability methods for high-value, cost-efficient offshore WIND) aims at pushing the state-of-the-art in the wind energy design and reliability prediction with advanced methods. It brings together a consortium combining universities and research organisations with industrial end-users. One of the objectives of this EU Horizon 2020 project is to enhance current load assessment methods tailored to the dynamics of large FOWT, realistically capturing complex phenomena such as fluid-structure interaction. The present work takes place within this project, focusing on wave-structure hydrodynamic interaction.

Focusing on floating systems, the classical methodology for the design of offshore structures is to employ a linear potential flow model for waves, assuming a perfectly rigid floater. This comes with the advantage of low computational cost, but with the assumption that the viscosity, as well as the vorticity of the flow, can be neglected. However, such effects may be important for thin elements of the floater, such as heave plates for instance. To overcome this shortcoming, it is convenient to add in the calculated loads a drag contribution (using a drag coefficient C_d) based on the Morison formulation, that usually provides a good representation of those effects. Many different simple geometries have already been tested and serve as guidelines for selecting appropriate C_d values. However, for more complex geometries involving a full 3D flow, the calibration of this drag coefficient might be difficult.

This hydrodynamic approach combining linear potential flow theory and empirical Morison formulation has been developed and widely validated for Oil & Gas platform design and is now applied to FOWT. However, the design constraints are quite different between those two fields: risks are lower in wind industry whereas cost optimization has to be pushed further in order to make renewable energies competitive. Thus, design tools performance should be reassessed in this new design context. Empirical coefficients (drag and added mass) of the Morison formulation are usually tuned based on existing database (from guides such as DNV-RP-C205 or basin tests). These databases should be revised in order to cover typical sizing and motions encountered with FOWT. Moreover, multiple sources of uncertainties can be emphasized in this current approach. First and foremost, the finite-dimension effect of the components of the structure that are not infinite nor 2D in real cases. Secondly, the assumed independence of the flow from the presence of the body, which is a core hypothesis of the Morison theory, might also be put into question. This is particularly true when a part of the body would be upstream and perturb the flow impacting the rest of the structure in a significant manner.

Nevertheless, this method could be fruitfully complemented by the Computational Fluid Dynamics (CFD) approach. Calibrating those coefficients more precisely thanks to CFD could help reducing the conservatism and consequently improve the design process. On top of that, other effects could be investigated with high-fidelity simulation tools, hence increasing the physical understanding of the floater hydrodynamics.

Great progress in recent years has shown the relevance of Numerical Wave Tanks (NWTs) approaches for FOWT. After finding some underestimation and discrepancies when calibrating drag coefficients [2], the OC6 project [3] has shown that it was possible to reproduce basin tests in regular and bichromatic waves on a fixed or free semi-submersible FOWT floater in waves with a level of uncertainty close to that encountered in experiments. Recent studies lead to promising methods to calibrate Morison's coefficients for FOWT purposes thanks to CFD [4]. Some improvements have also recently been reported, in particular regarding the drag coefficients of the elements close to the surface and of the heave-plates, in the case of the DeepCWind semi-submersible floater. The CFD simulations of this same floater also allowed the modification of the quadratic transfer functions (QTF) used in the engineering models, to obtain better results [5].

In this study, we restrict our attention to uncertainties associated with the determination of the Morison hydrodynamic coefficients (HCs) composed of drag C_d and inertia C_m terms for different Keulegan-Carpenter (KC) numbers, defined as the ratio of the amplitude of motion of a fluid particle by the dimension of the object, both in the same spatial direction:

$$\mathrm{KC} = \frac{U_m T}{D}, \tag{1}$$

where U_m is the flow velocity amplitude in the considered direction, T the wave period and D the characteristic object dimension in the same spatial direction.

The selected body is the complete floater designed by UMaine [6], shown in Figure 1, on which the objective will be to derive the HCs on different parts of the floater. We first set up two validation cases of simpler geometries, that resemble some parts of the UMaine floater, to validate the methodology and employed numerical models against experimental data and against each other. As a first step, the methodology and models will be validated against experiments compared together on simple shapes as follows:

1) a fully immersed infinite (2D) cylinder of rectangular cross-section [7] [8], presented in section IV,
2) a 3D piercing vertical circular cylinder, not extending down to the seabed [9] (not presented here for the sake of brevity).

Extensive comparisons have been made on those two simplified cases, both between the two CFD approaches used in this work and against experimental results.

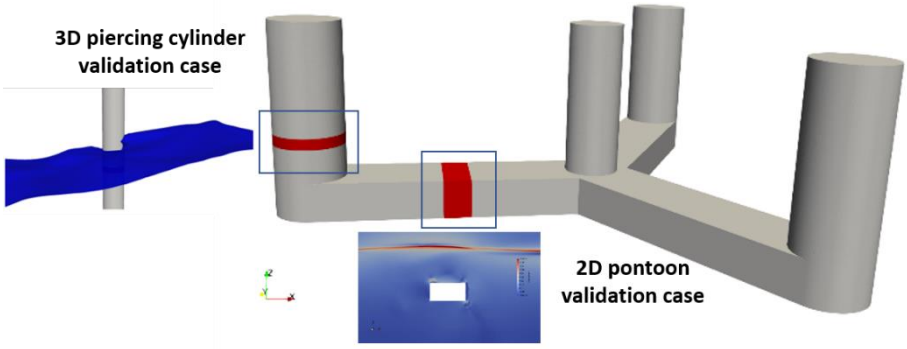

Figure 1. UMaine Floater sketch and the two presented validation cases of simpler geometries.

After these validation steps, the full floater shown in Figure 1 will be studied in different conditions with both CFD models.

The HCs are obtained thanks to a NWT set-up. Based on the Least Square method, a comparison between CFD forces and the Morison's empirical formulation is done. [7] has already proposed this method based on Morison's empirical formulation to extract HC obtained experimentally. [4] used a similar method replacing the experimental results with CFD forces.

II – CFD simulations tools

II – 1 neptune_cfd with an Immersed Boundary model (ncfd)

neptune_cfd is a 3D multi-field solver which was specifically developed for nuclear applications, but its field of application is growing with hydraulic, structure-wave interaction or naval applications. It is based on an Eulerian-Eulerian (two-fluid) approach with a single pressure [10] [11] [12] [13]. The discretization follows a 3D full-unstructured finite-volume approach, with a collocated arrangement of all variables. neptune_cfd is using inlet/outlet functions and HPC capabilities from the open-source single-phase CFD software code_saturne[1], used as pre-requisites.

Several turbulence models are available in neptune_cfd: a *k-ε* model with "linear production" [14] and an advanced Reynolds Stress turbulence Model, namely *Rij* -ε SSG [10] are used in the present work.

For the present Eulerian-Eulerian approach, a specific model, the Large Interface Model (LIM) [14], is used to deal with the free surface. It includes large interface recognition interfacial transfer of momentum (friction) [15].

A discrete forcing method (a variant of the Immersed Boundary method) is used to represent the solid on the mesh. The domain contains the structure, which is considered as a real part of the calculation domain thanks to a Time and Space Dependent Porosity (acting like a solid fraction) [16]. The idea is to reshape the cells crossed by the interface and to build specific schemes inside them to reconstruct wall properties. The main advantage of this method lies in the non-explicit representation of the structure. It is then possible to perform calculations on complex solid geometries using Cartesian grids. Further details can be found in [16].

To ensure a correct generation and absorption of the waves, a relaxation technique is used on a portion of the numerical domain. In these zones, a source term is added, to the momentum equation only, to drive the water velocity toward a target value: a theoretical propagative regular wave of a given amplitude and period at the inlet and a still water at the outlet. The theoretical wave is computed through a highly accurate non-linear model based on the so-called Stream Function theory. In addition, an inlet condition is implemented, to enforce the wave elevation from this same theoretical model. Together, those techniques prove to generate and absorb an accurate wave field, and are used in maritime studies such as [17].

II – 2 OpenFoam® model

Simulations of wave propagation with a fixed body or forced motion in still water have been performed with OpenFoam® with VOF (Volume of Fluid) approach [18]. In this solver, the phase function indicator called α is defined as the quantity of water per unit of volume in each cell. This means that if $\alpha = 1$, the cell is full of water, while if $\alpha = 0$, the cell is full of air. All the other values concern the air/water interface description. It is straightforward to calculate any of the properties of the fluid at each cell, just by weighting them by the VOF function. For example, the fluid density and the dynamic viscosity of the cell are computed respectively as:

$$\rho = \alpha\rho_{\text{water}} + (1-\alpha)\rho_{\text{air}}, \tag{2}$$

$$\mu_{\text{eff}} = \alpha\mu_{\text{water}} + (1-\alpha)\mu_{\text{air}} + \rho\nu_t, \tag{3}$$

where $\rho\nu_t$ denotes the turbulent viscosity which contributes to the effective dynamic viscosity μ_{eff}. If a laminar solution is sufficiently accurate, ν_t is set to zero. Otherwise, turbulent effects are incorporated in the RANS (Reynolds Averaged Navier-Stokes) equations by solving one or more additional transport equations, to yield a value for ν_t. In the VOF method the interface between air and water is tracked by solving an advection equation of the phase fraction field, namely the interface:

[1] www.code-saturne.org

$$\frac{\partial \alpha}{\partial t} + \nabla \cdot (\alpha u) = 0. \quad (4)$$

The *MULES* (Multidimensional Universal Limiter for Explicit Solution) method is used throughout this work to solve (4). For more details on the different approaches used, see [19]. Specific boundary conditions for the velocity, pressure and phase fraction fields are imposed on edges of the NWT using the waves2foam library [20], as illustrated in Figure 2. Concerning lateral boundary conditions, wall type conditions have been used. For 3D simulations, a large domain in *y* direction is necessary to limit reflection effects.

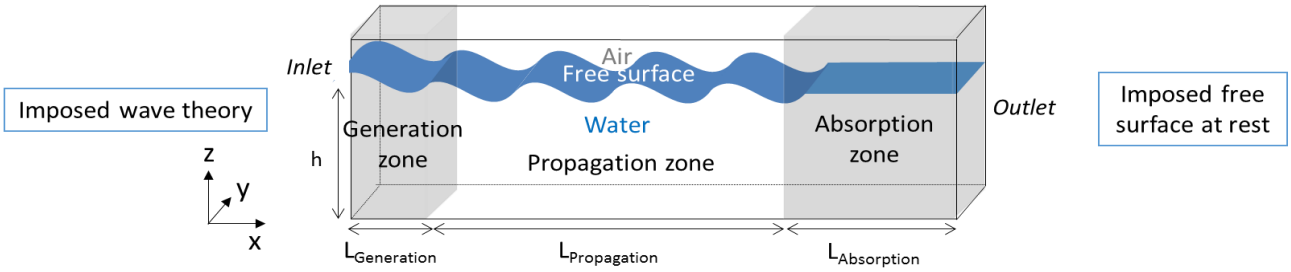

Figure 2. NWT illustrative sketch with waves2foam solver.

Different weighting functions within the relaxation zones have been introduced by [20]. In this study, only the exponential weighting function has been tested.

III – Extraction of the hydrodynamic coefficients

From a given discretized wave field and associated load time series, multiple strategies can be employed to extract the different HC, namely C_d and C_m, that model the loads *via* the so-called strip theory. In the most common formulation of Morison equation, the strip theory requires the knowledge of the relative velocity and acceleration of an object within a fluid:

$$F_{mx} = \rho V C_{mx} \dot{u}_x + \frac{1}{2} \rho S_x C_d u_x |u_x|, \quad (5)$$

where x is the direction of the load, u_x and $\dot{u}_x$ the relative velocity and acceleration of the object respectively, ρ the fluid density, V the volume of the object (or the part of the object), and S_x the projected surface of the object on a plane normal to the x axis.

From a given load series F_{xi}, extracted from a numerical simulation or an experiment, multiple solutions exist to extract C_d, C_m for which F_{mx} is the closest as possible to F_{xi} at every instant.

Two different methods of identification will be used here. The first one, presented in further detail in [8] or [21] is the minimisation of an L_2 error e between the modelled time series and the extracted one for N time instants:

$$e = \sum_{i=0}^{N} (F_{mx}(t = t_i) - F_{xi})^2. \quad (6)$$

This method will be denoted L2M hereafter (L_2 method).

The second method, denoted O3M (order 3 method) in the following, has been derived during this work and is an extension of the work of [22]. It is based on a Fourier expansion of (5) at the order 3. Assuming the form $u = a\omega\cos(\omega t)$, it is possible to write $u|u| \sim a^2\omega^2(0.849\cos(\omega t) + 0.169\cos(3\omega t))$. Thus, by identification:

$$C_{mx} = -\frac{F_{xs1}}{\rho V a \omega^2} \quad (7)$$

$$C_{dx} = \frac{\sqrt{F_{xc3}^2 + F_{xs3}^2}}{\frac{0.169}{2}\rho S_x a^2 \omega^2} \quad (8)$$

where F_{xci}, F_{xsi} are respectively the cosine and sine contributions of the i[th] order term, obtained through a Fourier decomposition of the load series F_{xi}.

In order to validate the models and methodologies, we first focus on cases of simple geometry, for which literature results are available.

IV – Fully immersed horizontal cylinder of rectangular cross-section

IV – 1 Presentation of the case

The test case presented in [8] [7] is selected. Note that a small difference in terms of aspect ratio (height/length of the rectangular cross-section) can be seen between the UMaine floater pontoons (0.56) and the selected test case that was experimentally studied (0.50). The experimental set-up as well as the studied test case are shown side-by-side in Figure 3.

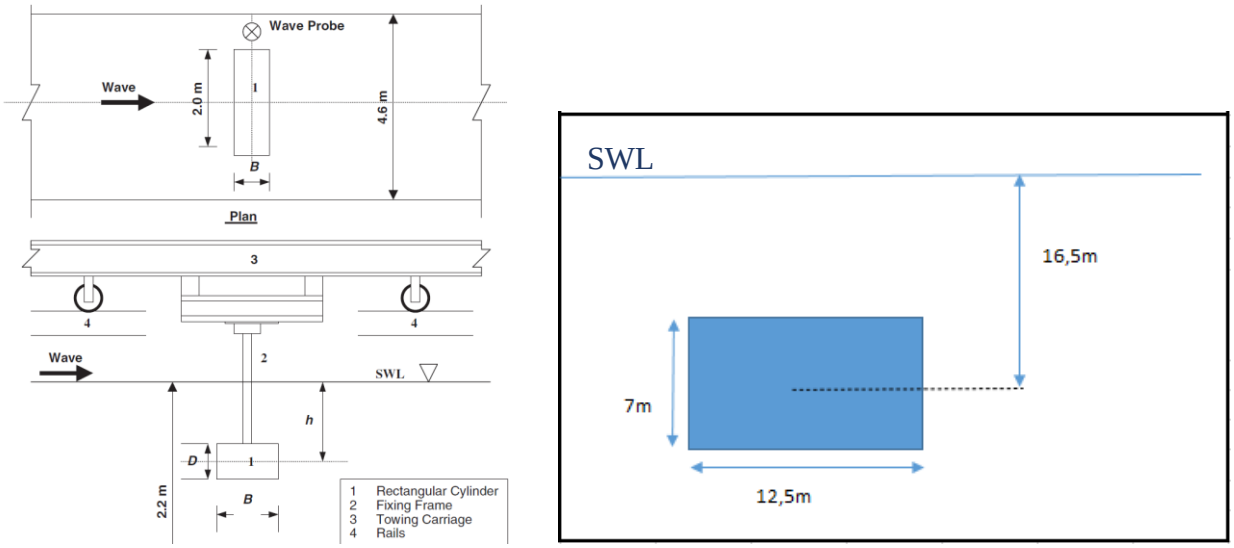

Figure 3. Experimental set-up from Venugopal in a towing tank [7] (left) and studied configuration (right) where the blue line is SWL.

IV – 2 Results

A set of 4 regular wave conditions were selected in this work (see Table 1). The objective was to cover a large range of KC number, known to largely impact the flow physics and thus the HC.

Table 1. Selected regular waves conditions where H is the wave height, T the wave period, h the water depth and λ the wavelength.

Case	H [m]	T [s]	h [m]	λ [m]	KC [-]
Wave 1	0.078	1.3	2.2	2.638	0.2
Wave 2	0.172	1.9	2.2	5.558	0.8
Wave 3	0.301	1.9	2.2	5.558	1.4
Wave 4	0.366	1.9	2.2	5.558	1.7

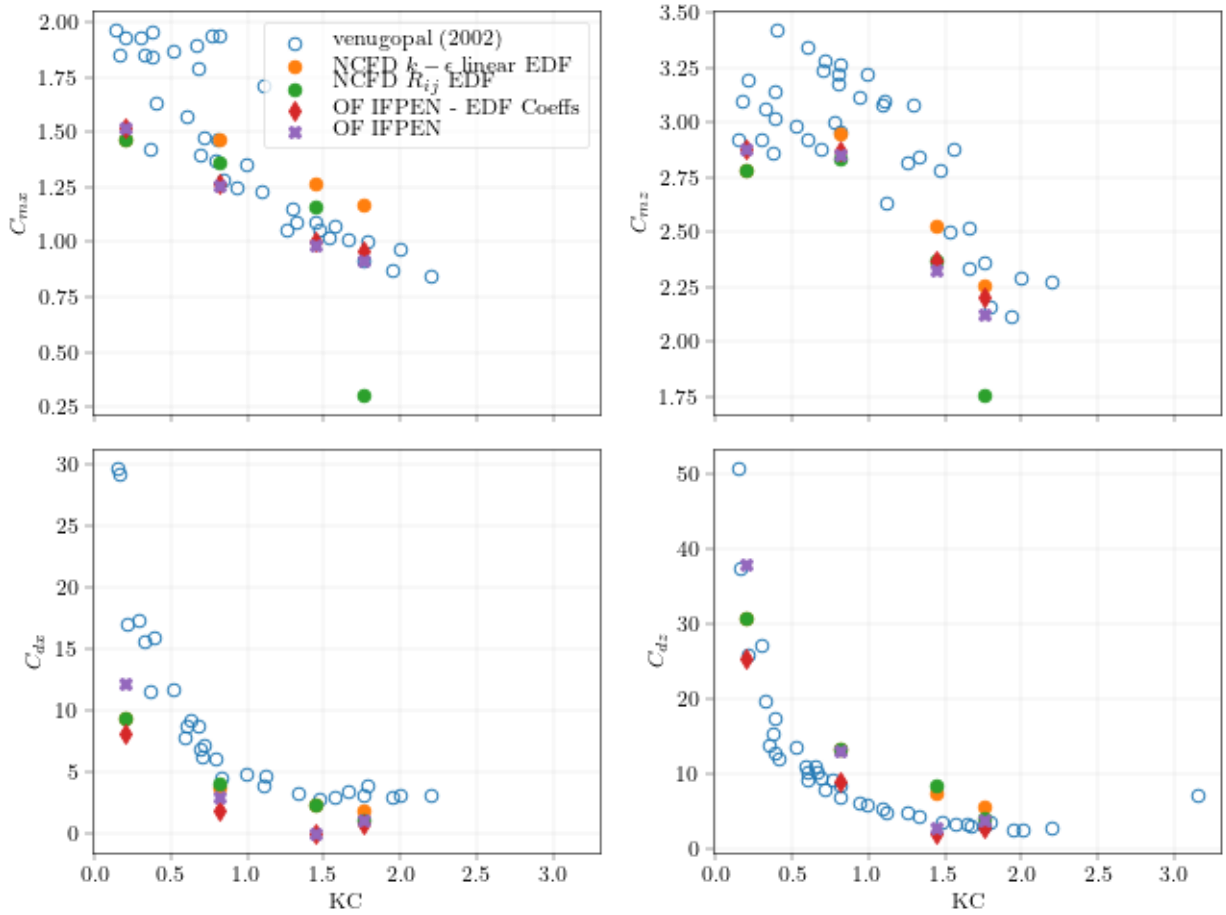

Figure 4. neptune_cfd (colored dots), OpenFoam® (cross and diamonds) results compared to Venugopal's experiments [7]. The HC extraction method is validated by applying the EDF method to the IFPEN load series (see text for details).

The final HC results for the four wave cases are presented in Figure 4. Each graph shows the variation of one-directional coefficient (C_m at the top and C_d at the bottom) at different levels of KC. This figure gives a good overview of the uncertainty obtained on the coefficients both experimentally and numerically. Blue circles (○) represent the Venugopal experiments [7], the remaining symbols correspond to the different CFD simulations. The filled circles represent neptune_cfd results with two different turbulence models ($k-\epsilon$ linear production: ● [14], and R_{ij}: ● [10]).

The choice of the theoretical kinematics of the incident wave field is of prime importance in the determination of the HC when the L2Mis applied (see (5) and (6)). While EDF uses a stream function method [23] to estimate the kinematics, IFPEN uses a Stokes theory of order 3 (✖). To assess that this difference is not of significant influence, a set of HCs has also been derived from the IFPEN load time series using the stream function kinematics (diamonds, ♦). Thus, both diamond and cross shapes correspond to extractions from OpenFoam® time series. Differences can only be denoted at small KC numbers, *i.e.* in regions dominated by inertia.

V –Full University of Maine floater, benchmark, results and discussions

Because the goal is to assess the capabilities of a CFD NWT at extracting up to local drag coefficients on a geometry of practical relevance, the UMaine floater was selected. A particular attention was devoted to five specific zones illustrated in Figure 5.

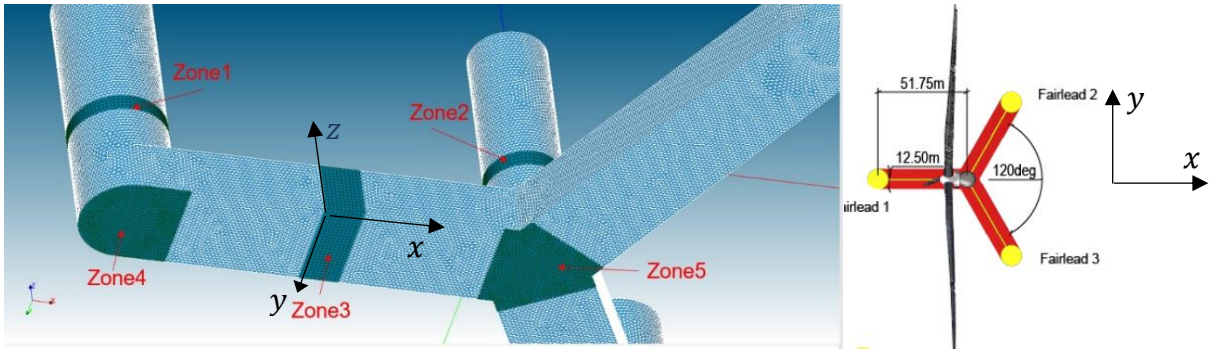

Figure 5. Representation of the 5 zones used to extract the Morison coefficients (left), and top-view of the UMaine floater (from [6])

Three load cases have been defined and are summarized in Table 2. They correspond to classical load cases used in the literature to derive HC. Other load cases have been studied but are not presented here for the sake of brevity.

Table 2. Benchmark cases to compare the Morison coefficients on each zone.

Wave Conditions			Imposed motion conditions			Horizontal Forces				Vertical Forces	
H [s]	T [s]	Orientation [deg]	Amplitude [m]	Period [s]	Direction [-]	KC - Zone 1	KC – Zone 2	KC – Zone 3	KC – Zone 4	KC – Zone 5	KC – Zone 3
6	10	0	-	-	-	1,18	1,48	0,78	1,39	1,39	1,39
-	-	-	3	10	Sway	1,51	1,88	1,51	-	-	-
-	-	-	3	10	Heave	-	-	-	2,69	2,69	2,69

V – 1 Forced sway motion analysis

A forced sway motion test case, on which the floater is forced to oscillate along the horizontal y axis in a fluid at rest is first set up in order to validate the two numerical models against each other on the full floater geometry. We first restrict our attention to the hydrodynamic loads on the central column (zone 2 on Figure 5), as well as its decomposition into HC.

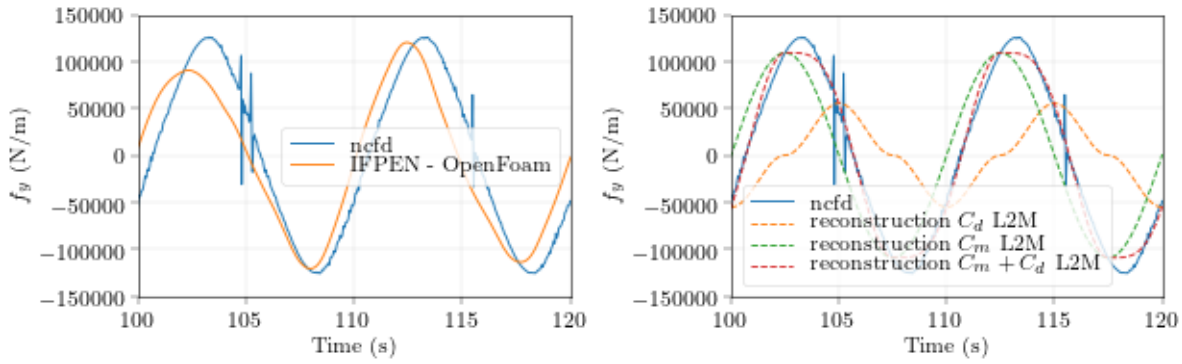

Figure 6. Time series of the hydrodynamic horizontal load applied on a horizontal slice of the central column (zone 2) predicted by neptune_cfd (EDF, solid line blue). On the left panel is added the OpenFoam® predictions (IFPEN, solid line, blue). Morison contributions of the neptune_cfd time series, computed with the L2M, are shown on the right panel (drag, mass and mass+drag).

Figure 6 depicts the different time series of the loads in this first benchmark case. While the time series of OpenFoam® and neptune_cfd are in relative agreement concerning the amplitude, a phase shift is denoted. That phase shift influences the computation of the Morison coefficients (shown in

Table 3) with the L2M: even the "best" – in the L_2 norm sense – set of coefficients is not appropriate to accurately model the horizontal loads obtained with neptune_cfd. A small phase shift error, compared to the "$\sin(\omega t)$" (phased with the relative acceleration of the object, in blue), leads to a large part of the time series being forwarded into the "$\cos(\omega t)\,|\cos(\omega t)|$" contribution (in orange), and thus to a significant overprediction of the drag coefficient ($C_d = 3.07$ for neptune_cfd). Note that a slight amplitude variation is observed between 102 and 112s on IFPEN time series, that could originate from a wall interaction effect caused by an insufficient damping zone in y axis (*i.e.*, the radiated wave field from the forced oscillations reflecting on the domain boundary). However, that effect does not impact the present analysis in a significant manner. Note that the obtained L2M C_d for the zone 5 predicted by neptune_cfd is negative, while OpenFoam predicts a value close to zero. This seems to question the validity of the Morison formulation hypothesis.

Table 3. Drag and Added-mass coefficients obtained with the L2M and the O3M (see section III)

	C_d		C_m	
method	L2M	O3M	L2M	O3M
OpenFoam®	1.07	1.45	1.07	1.08
neptune_cfd	3.07	1.36	1.14	1.07

However, it was denoted that shifting in time the load series before performing the L2M could affect the obtained drag coefficient in a significant manner: a shift of 4.5% of the period leads to a reduction of the C_d from 3.07 to 1.04 for neptune_cfd results. In this case, the Morison model can fit the "shifted" time series. This high sensitivity can be explained by the low contribution of the drag component in the total load.

To overcome this effect and obtain a reliable yet accurate drag coefficient, the method presented in section III, based on the norm of the third-order component of the load (O3M), is applied. It is thus not relying on the phase of the obtained series. With this method, the obtained drag coefficient is retrieved at a value closer to the expectations and the C_d extracted from OpenFoam® and neptune_cfd agree more closely (1.36 and 1.45 respectively).

Note that a high frequency signal is perturbating the neptune_cfd load series, which is linked to the cell shift of the porosity field, thus leading to increased difficulty to retrieve the object faces at some time steps. The obtained HC are, however, relatively close as the high frequencies are filtered out by the HC identification process, with both methods. For this reason, a high-frequency filter is applied on the temporal series of loads obtained with neptune_cfd, and only those filtered temporal series will be shown hereafter.

V – 2 Forced heave motion analysis

The floater is forced into a heave motion of period 10 s and amplitude 3 m. Applying the same methodology, the predicted loads are extracted from the simulations on the different zones of interest (presented in Figure 5). Time series of the vertical loads are shown in Figure 7 for the zone 3 and in Figure 8 for the zones 4 and 5. A good agreement between the OpenFoam® and neptune_cfd predictions is consistently denoted. Table 4 presents the different HC obtained from the presented time series.

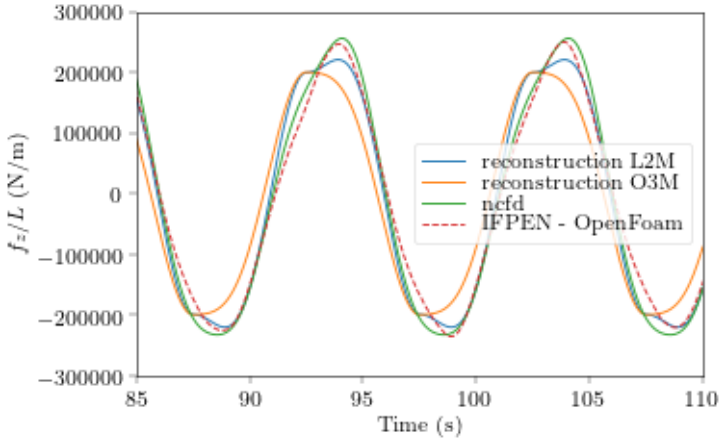

Figure 7. Vertical load series predicted by OpenFoam® and neptune_cfd on the pontoon (zone 3), for a forced heave motion. The load is divided by the horizontal length of the considered zone. Reconstructions of the load series are shown using the values given in Table 4 (neptune_cfd reconstruction).

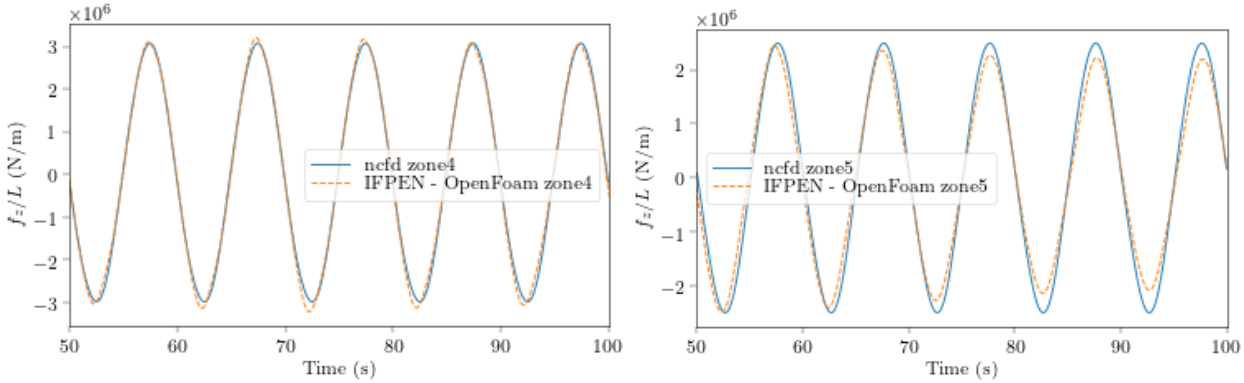

Figure 8. Time series of the hydrodynamic vertical load applied on zones 4 (left) and 5 (right), predicted by OpenFoam® (IFPEN) and neptune_cfd (EDF) for a forced heave motion of the structure.

Table 4. Drag and added mass coefficients obtained with the different identification methods, for the zones 3, 4 and 5

Coefficient	C_d		C_d		C_d		C_m	
Zone	Zone 4		Zone 5		Zone 3			
Identification method	L2M	O3M	L2M	O3M	L2M	O3M	L2M	O3M
OpenFoam®	1.15	1.54	0.08	1.43	6.95	10.46	1.76	1.01
neptune_cfd	0.89	0.89	-0.72	0.99	6.93	3.96	1.87	1.88

Despite a good agreement in terms of temporal load series, the obtained HC with both the O3M and the L2M do not give a very satisfactory time series approximation, as can be denoted on Figure 7. Note that for the zones 4 and 5, the C_m value is not completely meaningful, as we do not have any full "volume" being subjected to a given relative kinematics. It is therefore not presented here.

V – 3 Incident regular wave field

The same analysis can be performed on the case of incident regular waves of period 10 s and height $H = 6$ m. In this context though, the O3M cannot be applied, because it is expected that not

only the drag from the order 1 kinematic generates third order loads, but also the order 3 part of the kinematics directly.

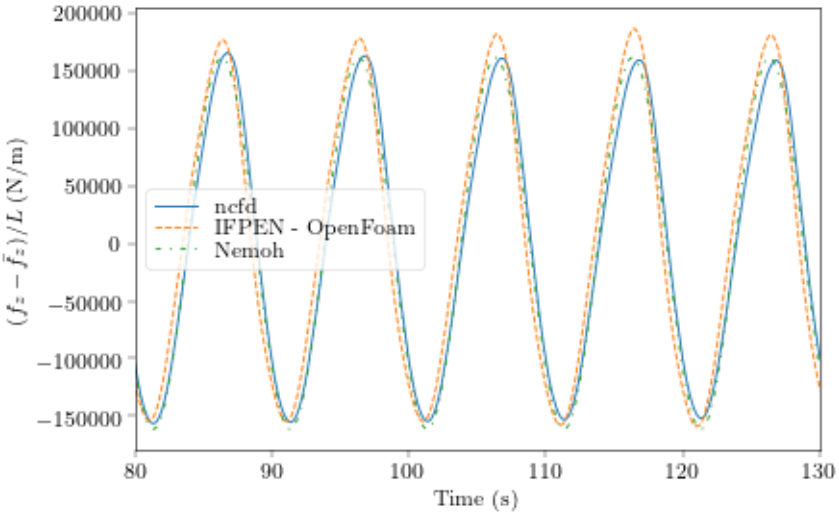

Figure 9. Predicted vertical wave load time series on a portion of the pontoon (zone 3) with OpenFoam®, neptune_cfd, and Nemoh (linear potential model, no drag contribution).

Figure 9 shows the time series for the vertical load on zone 3. In addition to the two CFD models, a simulation has been computed with Nemoh [24] (BoEM linear potential model). Because it uses the potential hypothesis, no drag can be predicted. With this model, the obtained loads are thus completely in phase with the particle acceleration (under the strip theory assumption, which is supposed to be almost applicable given the floater geometry). While we can notice a discrepancy in terms of obtained amplitude between OpenFoam® and neptune_cfd, a relative agreement is found in phasing between the three models. Concerning the amplitude difference, the higher maximum efforts observed with OpenFoam® could come from differences on close body mesh strategies and the different turbulence modelling used by each code. Because a phase shift can be observed between neptune_cfd and OpenFoam® predictions, the latter being more in phase with the results of Nemoh, it can be foreseen that a lower drag coefficient will be obtained with OpenFoam®. In that case, we indeed predict a $C_d = 4.80$ from the OpenFoam® results and a $C_d = 13.33$ from the neptune_cfd results, using the L2M. Note that the C_m coefficients, responsible of the large majority of the loads here, are in better agreement, with 3.02 and 2.68 respectively. This analysis once again demonstrates the very high sensitivity of the drag coefficient to a phase shift in those range of conditions.

The same agreement can be found in the horizontal load series applied on the two columns of the floater, depicted in Figure 10.

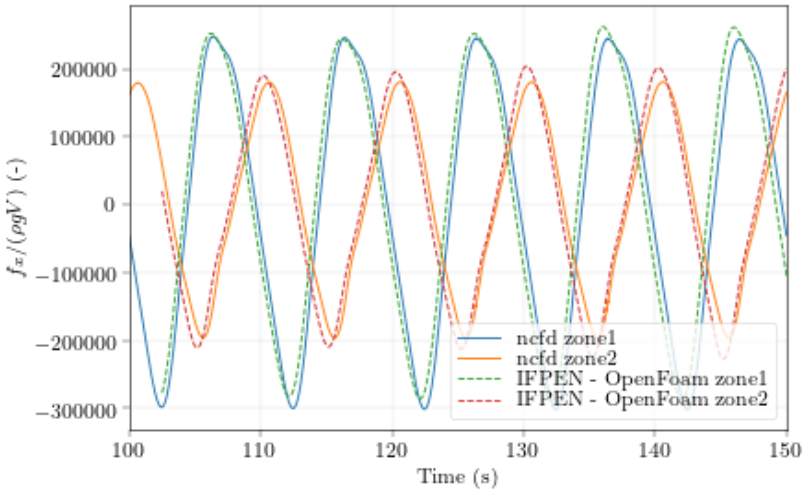

Figure 10. Predicted horizontal wave load time series on a portion of the central and front columns (zones 1 & 2). OpenFoam®, neptune_cfd.

Table 5. Drag and Added-mass coefficients obtained with the L2M for all considered zones in the benchmark case, incident wave of period 10 s and wave height of 6 m.

	Zone 1		Zone 2		Zone 3		Zone 4		Zone 5	
	C_{mx}	C_{dx}	C_{mx}	C_{dx}	C_{mz}	C_{dz}	C_{mz}	C_{dz}	C_{mz}	C_{dz}
OF	2.23	-2.03	2.67	3.03	3.02	4.80	-	6.06	-	-0.89
ncfd	2.20	5.22	2.23	7.11	2.68	13.33	-	8.36	-	-7.89

V – 4 Discussion

While an overall fair agreement in terms load time series can be denoted between the two CFD codes, a relatively significant dispersion in the fitted HC can be observed (see *e.g.* Table 5). However, it can be noted that larger KC values usually lead to better agreement between methods. An error is associated with the CFD models themselves, due to the different approximations and models (domain discretization, spatial scheme discretizations, temporal discretization, turbulence models, *etc.*). This error could be roughly estimated to be less than 3~5% and could impact the obtained temporal series both *via* a phase shift or through the load amplitude or shape. In addition, an error might be introduced in the post-treatment step, within the CFD code, during the computation of the loads from the different fields. This is, for example the case of the neptune_cfd porosity method, which can present irregular time series due to a shift in the geometrical definition of delimited volume of the floater. Among the two methods of HC extraction:

- The O3M will output HC based on the overall shape (third order of the load series) and thus relies on a small contribution to the total load series amplitude. Moreover it is also relatively sensitive to spurious effects on the load computation. On the other hand, an error on the phase of the signal will not modify the obtained C_d with this method.
- The L2M is on the contrary not largely impacted by spurious effects, or an overall error in shape or in amplitude of the load time series, but it relies in background on the phase shift between the velocity acceleration and the obtained loads and is very sensitive to this value.

Given the different obtained load series and their associated small errors, the goal is to fit a Morison-type representation that we consider to be valid for simple shapes in oscillatory or orbital relative fluid displacement. In the case of incident waves, the range of validity is also ensured for small objects compared to the oscillation amplitude of a fluid particle, *i.e.* when the drag and inertia dominates over the diffraction effects (approximately $\frac{\pi D}{\lambda} < 0.5$, where D is the object characteristic dimension, and λ the wavelength). The underlying assumption is that the object does not perturb the fluid kinematics in a significant manner. This hypothesis is of course questionnable in our study,

because the flow is 3D and the different parts of the full floater diffract (incident regular waves) or radiate (forced motions) waves that will modify the relative fluid kinematics in the considered zone.

VI – Conclusions and future works

After a validation of the code and methodologies on cases of simple geometry against experimental results, the two CFD tools are used on a complete semi-submersible FOWT floater. It is shown that valuable results can be drawn from the use of such methodology, even though a special care must be taken in the modelling of the obtained load time series with a set of hydrodynamic coefficients (HC).

Two different HC identification methods are used. The "order 3" method (O3M) relies on the correct computation of a term of small relative amplitude (the third-order component of the loads), which can also be prone to errors. On the other hand, the L2 method (L2M) relies on the correct computation of the phase -which has never shown to exceed 3 to 4% of error- but exhibits a large sensitivity to any phase shift error. This phase shift seems to be higher in the neptune_cfd results and makes its results more sensitive to the HC identification method. The OpenFoam® results sometimes exhibit low frequencies contributions, which do not seem to affect too much the determination of the HC.

The results presented highlight that large uncertainty can be obtained in the determined drag coefficients, mainly due to the fitting procedures which are either sensitive to phase shift or spurious effects in the CFD load time series. Note that this is amplified by the fact that loads on the studied floater are dominated by inertial effects, with small contributions of the drag term. As many floating foundations can experience similar issues, it is worth trying to quantify the dispersion obtained on drag coefficients in that situation.

Possible future studies and extensions could encompass two main axes:

- First and foremost, the convergence studies in both mesh and time discretizations could be pushed further, especially in the case of forced motions, where the relative kinematics are explicitly enforced. The incident wave cases add another source of error in phase shift, related to the wave propagation simulation. This phase shift was shown to play a determinant role in the determination of the drag coefficient. In these incident wave cases, it is also possible to simulate the same problem on the same meshes without the body to extract the real kinematics (or phase shift) at the location of the zones on interest.
- Then, and especially in neptune_cfd, a better method of local wave load extraction could be implemented for two main reasons: to remove the spurious effects on the load series, but also to better represent all types of zones and shapes. The simulations could also be refined by assessing the effect of not using absorber zones in the *x* direction for the sway motion case.

Acknowledgements

This study is supported by the Hiperwind project funded by the European Union's Horizon 2020 Research and Innovation Program under Grant Agreement No. 101006689. The support is greatly appreciated. The authors also thank Pauline Bozonnet (IFPEN) for her contribution in the project.

References

[1] European Commission, "COM(2020) 741 Final," 19 November 2020. [Online]. Available: https://eur-lex.europa.eu/legal-content/EN/TXT/PDF/?uri=CELEX:52020DC0741&rid=1.

[2] A. N. Robertson, S. Gueydon, E. Bachynski, L. Wang, J. Jonkman, D. Alarcón, E. Amet, A. Beardsell, P. Bonnet, B. Boudet, C. Brun, Z. Chen, M. Féron, D. Forbush, C. Galinos, J. Galvan, P. Gilbert, J. Gómez, V. Harnois, F. Haudin, Z. Hu, J. L. Dreff and al., "OC6 Phase I: Investigating the underprediction of low-frequency hydrodynamic loads and responses of a floating," in *Journal of Physics: Conference Series. The Science of Making Torque from Wind (TORQUE 2020)*, 2020.

[3] L. Wang, A. Robertson, J. Jonkman, Y.-H. Yu, A. Koop, A. B. Nadal, H. Li, E. Bachynski-Polić, R. Pinguet, W. Shi, X. Zeng, Y. Zhou, Q. Xiao, R. Kumar, H. Sarlak, E. Ransley and al., "OC6 Phase Ib: Validation of the CFD predictions of difference-frequency wave excitation on a FOWT semisubmersible,," *Ocean Engineering*, vol. 241, p. 110026, 2021.

[4] C. Clément, P. Bozonnet, G. Vinay, P. Pagnier, A. B. Nadal and J. Reveillon, "Evaluation of Morison approach with CFD modelling on a surface-piercing cylinder towards the investigation of FOWT Hydrodynamics," *Ocean Engineering, Volume 251,* vol. 251, p. 111042, 2022.

[5] L. Haoran and E. E. Bachynski-Polić, "Validation and application of nonlinear hydrodynamics from CFD in an engineering model of a semi-submersible floating wind turbine," *Journal of Marine Structures*, vol. 79, p. 103054, 2021.

[6] C. Allen, A. Viscelli, H. Dagher, A. Goupee, E. Gaertner, N. Abbas, M. Hall and G. Bartner, "Definition of the UMaine VolturnUS-S Reference Platform Developed for the IEA Wind 15-Megawatt Offshore Reference Wind Turbine," National Renewable Energy Lab. (NREL), Golden, CO (United States); Univ. of Maine, Orono, ME (United States), Univ. of Maine, 2020/07/01.

[7] V. Venugopal, K. S. Varyani and N. D. Barltrop, "Wave force coefficients for horizontally submerged rectangular cylinders," *Ocean Engineering*, vol. 33, no. 11, pp. 1669-1704, 2006.

[8] V. Venugopal, Hydrodynamic force coefficients for rectangular cylinders in waves and currents, Glasgow, Scotland: University of Glasgow, 2002.

[9] C. Stansberg, Comparing ringing loads from experiments with cylinders of different diameters—an empirical study, United Kingdom: U.S. Department of Energy, 1997.

[10] S. Mimouni, F. Archambeau, M. Boucker, J. Lavieville and C. Morel, "A second order turbulence model based on a Reynolds stress approach for two-phase boiling flow. Part 1: Adiabatic to the ASU-annular channel case.," *Nuclear Engineering and Design*, vol. 240, no. 9, pp. 2233-2243, 2010.

[11] J. Delhaye, Thermal-hydraulics of two-phase systems for industrial design and nuclear engineering, Hemisphere and McGraw Hill, 1981.

[12] P. Coste, "A Large Interface Model for two-phase CFD," *Nuclear Engineering and Design*, vol. 255, pp. 38-50, 2013.

[13] M. Ishii and T. Hibiki, Thermo-fluid Dynamics Theory of two-Phase Flow, Eyrolles: Collection de la direction des Etudes et recherches d'Electricité de France, 1975.

[14] V. Guimet and D. Laurence, "A linearized turbulent production in the k-ε model for engineering applications," *Proceedings of the 5th international symposium on engineering turbulence modelling and measurements*, pp. 157-166, 2002.

[15] P. Coste, J. Pouvreau, C. Morel, J. Laviéville, M. Boucker and A. Martin, "Modeling turbulence and friction around a large interface in a three-dimension two-velocity eulerian

code," in *Proceedings - 12th International Topical Meeting on Nuclear Reactor Thermal Hydraulics, NURETH-12*, 2007.

[16] W. Benguigui, A. Doradoux, J. Lavieville, S. Mimouni and E. Longatte, "A discrete forcing method dedicated to moving bodies in two-phase flow," *International Journal for Numerical Methods in Fluids,* vol. 88, no. 7, pp. 315-333, 2018.

[17] M. Benoit, W. Benguigui, M. Teles, F. Robaux and C. Peyrard, "Two-Phase CFD Simulation of Breaking Waves Impacting a Coastal Vertical Wall with a Recurved Parapet," in *The 32nd International Ocean and Polar Engineering Conference*, Shanghai, China, 2022.

[18] C. Hirt and D. Nichols, "Methods for Calculating Multi-Dimensional, Transient Free Surface Flows Past Bodies," in *Proc. Of the First International Conference on Numerical Ship Hydrodynamics*, Gaithersburg, Maryland, October 20-23, 1975.

[19] L. Gamet, M. Scala, J. Roenby, H. Scheufler and J.-L. Pierson, "Validation of volume-of-fluid OpenFOAM® isoAdvector solvers using single bubble benchmarks," *Computers & Fluids,* vol. 213, p. 104722, 2020.

[20] N. G. Jacobsen, "waves2Foam Manual Technical Report," August 2017. [Online]. Available: https://www.researchgate.net/publication/319160515_waves2Foam_Manual.

[21] F. Robaux, Numerical simulation of wave-body interaction: development of a fully nonlinear potential flow solver and assessment of two local coupling strategies with a CFD solver, Marseille: Aix-Marseille Université, 2020.

[22] S. Arai, "Forces on and flows around a horizontal rectangular cylinder submerged in regular waves," in *Third International offshore and polar engineering conference*, Singapore, 1993.

[23] R. Dean, "Stream function representation of nonlinear ocean waves," *Journal of Geophysical Research,* vol. 70, no. https://doi.org/10.1029/jz070i018p04561, p. n° 18 4561-72., septembre 1965.

[24] A. Babarit and G. Delhommeau, "Theoretical and numerical aspects of the open source BEM solver NEMOH," in *11th European Wave and Tidal Energy Conference (EWTEC2015)*, Nantes, France, 2015.